King Saud University

Arabian Journal of Chemistry

www.ksu.edu.sa
www.sciencedirect.com

ORIGINAL ARTICLE

Green synthesis of platinum nanoparticles by *Nymphaea tetragona* flower extract and their skin lightening, antiaging effects

Yisen Zhang [a,b], **Shuo Cheng** [a], **Huiling Jia** [a], **Juanjuan Zhou** [a], **Jinfeng Xi** [a], **Jun Wang** [a], **Xue Chen** [a,*], **Lifang Wu** [a,b,c,*]

[a] *The Center for Ion Beam Bioengineering & Green Agriculture, Hefei Institutes of Physical Science, Chinese Academy of Sciences, Hefei 230031, Anhui, China*
[b] *School of Basic Medical Sciences, Anhui Medical University, Hefei 230032, Anhui, China*
[c] *Zhongke Taihe Experimental Station, Taihe 236626, Anhui, China*

Abstract Platinum nanoparticles (PtNPs) were green synthesized by using chloroplatinic acid (H_2PtCl_6) as raw material and *Nymphaea tetragona* (*N. tetragona*) flower extract as the capping and reducing agents to improve skin health. Size-tunable PtNPs were obtained by volume ratios of the initial H_2PtCl_6/*N. tetragona* of 1:1 and 1:4, in which PtNPs prepared by the ratio of 1:1 and 1:4 was defined as L1-PtNPs and L4-PtNPs. Their characterizations were investigated by UV–visible spectroscopy, TEM, XRD and FTIR spectroscopy. TEM image analysis showed the particles were well dispersed with the average particle diameters of L1 and L4-PtNPs were 4.04 ± 1.31 nm and 2.01 ± 0.80 nm, respectively. The synthesized PtNPs showed effective antioxidant property and anti-tyrosinase activity *in vitro*. And further experiments exclaimed that PtNPs can significantly inhibit tyrosinase activity and UVB-induced melanin biosynthesis in A375 cells. This study also revealed PtNPs can promote collagen I biosynthesis in HFF-1 cells by activating the TGF-β/Smad pathway. This research showed the potential efficacy of PtNPs in the skin field and provided evidence for people to consider applying PtNPs to skin protection.

* Corresponding authors.
E-mail addresses: xuechen1028@ipp.ac.cn (X. Chen), lfwu@ipp.ac.cn (L. Wu).
Peer review under responsibility of King Saud University.

Production and hosting by Elsevier

1. Introduction

In recent years, the application of platinum nanoparticles (PtNPs) in the biomedical field has received extensive attention. For example, PtNPs have been used to treat oxidative stress-related diseases and biomarkers (Samadi et al., 2018; Pedone et al., 2017; Al-Qudah et al., 2022). In addition, PtNPs have been approved as additives in consumer products and cosmetics (Pedone et al., 2017).

Traditional physical and chemical methods for the synthesis of metal nanoparticles (NPs) include vapor deposition, chemical reduction, pyrolysis, sol gel, laser ablation, etc (Jiao et al., 2021). However, these methods are harsh and energy-consuming. Harmful chemicals are used as sealants and reducing agents, and the remaining unreacted chemicals and dangerous by-products may be adsorbed on the surface of NPs (Jiao et al., 2021; Zheng et al., 2013; Chaudhary et al., 2019). Therefore, NPs produced by the above methods are not suitable for biomedicine, health and beauty applications. In order to address these shortcomings and avoid using hazardous reducing agents, the focus of this field has shifted to biosynthetic NPs by green biological methods, which employ bacteria, fungi, enzymes, plants and algae to produce NPs (Alvarez et al., 2016; Gahlawat and Choudhury, 2019; Siddiqi and Husen, 2016; Khan et al., 2018; Mondal et al., 2021). These biosynthetic PtNPs offer multiple advantages for pharmaceutical and biomedical applications due to its biocompatibility, environmental friendliness and higher cost-effectiveness (Jiao et al., 2021; El-Seedi et al., 2019). The synthesis of metal NPs by microorganisms can be divided into intracellular synthesis and extracellular synthesis. However, subsequent processing of intracellular biosynthetic NPs is usually arduous, and the microorganisms used for extracellular biosynthesis of NPs must be widely screened (Huang et al., 2009). Biosynthesis of metal NPs by living plants, plant extracts and phytochemicals has attracted more and more concern as an easy and beneficial alternative method for extracellular biosynthesis of metal NPs (Zheng et al., 2013). The green method of synthesizing metal NPs by plant is not only non-toxic and fast, but also the shape and size of the synthesized NPs are more controllable than that by microbial method (Bhardwaj et al., 2020). In addition, plants show excellent reducing and stabilizer effects in the synthesis of metal NPs (Siddiqi et al., 2018). The existence of flavonoids, protein amine residues and carboxylic acids in plants are the reasons why Platinum ions are reduced to PtNPs (Castro et al., 2015). Not only that, the abundant secondary metabolites and phytochemicals in plants play important roles in antibacterial, anti-inflammatory, anti-cancer and antioxidant activity (Zeng et al., 2013). Currently, *Cochlospermum gossypium Diopyros kaki* leaf and peppermint leaf extracts have recently been used to green synthesize PtNPs (Song et al., 2010; Yang et al., 2017; Venu et al., 2011). Studies have reported that PtNPs synthesized by peppermint leaf extract polyphenols reduce the viability of HCT116 cells at minor concentration (IC_{50} = 20 μg/mL), and PtNPs biosynthesized by *Tragia involucrata* leaf extract displayed in a dose-dependent manner on antioxidant activities and the activities were superior to the leaf extract (Yang et al., 2017; Selvi et al., 2020). However, there are few studies on the biological effects of PtNPs in the skin field.

N. tetragona, distributed in tropical regions around the world, contains phenols, flavonoids, tannins, alkaloids, anthraquinones, saponins, heart glycosides and other bioactive ingredients, which are equivalent to anti-diabetic, anti-inflammatory, collagen deposition and whitening (Chowdhury et al., 2021; Hsu et al., 2020; Rajagopal and Sasikala, 2008; Mukherjee et al., 1997). Although the various medicinal properties and active substances of this plant have been extensively studied, to our knowledge, there is no evidence that *N. tetragona* extract is used to green synthesize PtNPs and investigated its biological effect in the skin field. In this research, well-dispersed and stable PtNPs were green synthesized by *N. tetragona* extract as the capping and reducing agents. Additionally, the effects of prepared PtNPs on antioxidant activity, anti-tyrosinase activity and collagen synthesis were evaluated.

2. Materials and methods

2.1. Materials

Antibodies against type I collagen (collagen I, ab260043), transforming growth factor-beta (TGF-β, ab179695), Smad3 (ab208182) and p-Smad3 (ab52903) were obtained from Abcam (Cambridge, MA, USA). The antibody to β-actin was purchased from Abways (Shanghai, China). The secondary antibody was purchased from Jackson ImmunoResearch La boratories (USA). High-sugar DMEM was obtained from BasalMedia (Shanghai, China). Fetal bovine serum (FBS) was obtained from ShuangRu Biotech (LON-SERA, Shanghai, China). Penicillin streptomycin mixed solution (Penicillin 10000 U/mL and Streptomycin 10000 μg/mL) was obtained from Solarbio (Beijing, China). All other chemicals and reagents used in the study were analytical grade.

2.2. Preparation of N. tetragona extract

The *N. tetragona* flower sample (100 g) was blended with 95% ethanol solvent (1000 mL), extracted at 25 °C for 3 h, then centrifuged at 10000 rpm for 20 min, and the supernatant was collected. The residue was further extracted twice with 95% ethanol (500 mL) at 25 °C for 3 h. The ethanol extract solution was evaporated at 50 °C by rotary evaporator, and then redissolved in double distilled water for evaporation under reduced pressure at 40 °C until complete dryness and stored at −20 °C. Finally, 1 g of *N. tetragona* extract was added to 20 mL double distilled water for dissolution, centrifuged at 10000 rpm for 10 min, and the supernatant was taken for using.

2.3. Synthesis of PtNPs

H_2PtCl_6 (50 mM) of 2 mL and *N. tetragona* extract (50 mg/mL) were prepared in two conical flasks at volume ratios of 1:1 and 1:4, and the final volume was adjusted to 20 mL with double distilled water. The mixed solutions were placed on magnetics stirrer heated and stirred for 1 h, then stopped heating and continue stirred for another 30 min. After the reaction, the mixed solutions were placed at 25 °C for 30 min and centrifuged at 12000 rpm for 20 min. The precipitates were collected, re-suspended in distilled water and centrifuged at 12000 rpm for 20 min. Finally, the precipitates were redissolved in double distilled water and filtered by 0.22 μm membranes, and then utilized for later characterizations.

2.4. Determination of PtNPs concentration

The synthesized PtNPs aqueous solution of 50 μL was added to 4950 μL nitric acid overnight for nitrification. The nitrated solution was evaporated and redissolved in 5 mL double distilled water. L1-PtNPs and L4-PtNPs solution were filtered through FitMax Syringe Filter (13 mm 0.22 μm PTFE 100/pk), and platinum ions concentration was determined by Inductively coupled plasma mass spectrometer (ICP-MS, X SERIES II, USA).

2.5. Characterization of PtNPs

The reaction solution was scanned periodically by ultraviolet spectrophotometer (ScanDrop, Analytikjena, Germany) oper-

ated in the range of 200–729 nm to confirm the formation of PtNPs. The aqueous solution of NPs was freeze-dried by freeze dryer for approximately 24 h. Then, the dry samples were studied by X-ray diffraction spectroscopy (XRD, SmartLab, Japan) to acquire the composition and structure of the synthesized metal nanoparticles. SmartLab Guidance was used to record the data obtained from operation at 9 kW. The dry samples were examined at 4°/min in the range of 2θ from 10° to 90°. TEM (JEM-2100F, Japan) with XFlash 5030 T X-ray energy spectrometer was utilized to evaluate the morphology and size of the synthesized PtNPs. Fourier transform infrared spectroscopy (FTIR, Nicolet Is5, USA) was used to identify the bio-reductive compounds that led to the success of the reaction. A Bruker Tensor 27 system performed at range of 500–4000 cm^{-1} was used to acquire spectrums.

2.6. Antioxidant activity in vitro

2.6.1. Ferric reducing antioxidant power (FRAP) method

Newly prepared FRAP reagent consisted of acetic acid buffer (300 mM, pH = 3.6), TPTZ solution (10 mM) and $FeCl_3$ solution (20 mM). FRAP working solution was prepared freshly by commixing acetic acid buffer, TPTZ, and $FeCl_3$ solution at 10:1:1. In short, 500 μL of FRAP working solution and 500 μL of PtNPs solution with different concentrations were mixed and reacted at 37 °C for 10 min. The absorbance of reacted solution at 593 nm was noted by ScanDrop. Trolox was performed as positive control. IC_{50} value was demarcated as an efficacious concentration of scavenge 50% free radicals. FRAP-scavenging activity was calculated according to the formula below:

$$Scavenging ability(\%) = (A_1 - A_0) \times 100$$

where A_1 and A_0 are the absorbance values after the reaction between the PtNPs samples and blank control.

2.6.2. ABTS-Scavenging activity method

Stock solution of ABTS•+ was composed of mixing 140 mM ABTS and 40 mM potassium persulfate prepared in double distilled water. And stock ABTS•+ solution was diluted 20 times with PBS (pH = 7.4) to use. Briefly, 500 μL of ABTS• + working solution and 500 μL of PtNPs solution with different concentrations were mixed and reacted in the dark at 25 °C for 10 min. The absorbance of reacted solution at 414 nm was noted by ScanDrop. Trolox was performed as positive control. IC_{50} value was demarcated as an efficacious concentration of scavenge 50% free radicals. ABTS-scavenging activity was calculated according to the formula below:

$$Scavenging ability(\%) = (1 - A_1/A_0) \times 100$$

where A_1 and A_0 are the absorbance values after the reaction between the samples and blank control.

2.7. Determination of mushroom tyrosinase activity

Samples of different concentrations (0, 2, 5, 8 and 10 μg/mL) were made up to 100 μL by 0.1 M sodium phosphate buffer (pH = 6.8), then 50 μL mushroom tyrosinase (Sigma-Aldrich, St. Louis, MO, USA) solution (100 U/mL) were added. After mixing, incubated at 37 °C in the dark for 10 min. Then, 200 μL of levodopa (1 mg/mL) was put in

and the reaction was dark at 37 °C for 30 min. The absorbance of reacted solution at 475 nm was read on ScanDrop. The percentage of tyrosine activity and IC_{50} values were calculated according to the following formula:

$$Tyrosinase Activity(\%) = (T - T_0)/(C - C_0) \times 100$$

where T, T_0, C and C_0 were the absorbance values of the samples, sample control, control, and control blank, respectively.

2.8. Cell culture and cell viability

A human melanogenic cell line (A375) and a human skin fibroblast cell line (HFF-1) were cultured in High-sugar DMEM, supplemented with 10% FBS, 1% Penicillin streptomycin mixed solution in humidified incubator with 5% CO_2 at 37 °C. The cells were sub-cultured every 2 days to maintain logarithmic growth.

The toxicity of the PtNPs was measured using Cell Counting Kit-8 (MA0218-5, Meilunbio, Dalian, China). Briefly, A375 cells (2.0×10^3 cells/well) and HFF-1 cells (3.0×10^3 cells/well) were plated in 96-well flat-bottom culture plates. After incubated for 24 h and adhere to the wall, samples with different concentrations were added. With an additional culture for 24 h at 37 °C in incubator, cells were washed with phosphate-buffered saline (PBS) followed by the additional 100 μL of High-glucose DMEM medium (containing 10% CCK-8 solution) into every well and continued to incubate for 4 h at 37 °C. The absorbance at 450 nm was noted every hour by a microplate reader (PL-9602; PERLONG, Beijing, China). Cell viability was calculated according to the equation below:

$$Cell viability(\%) = (A_1/A_0) \times 100$$

where the absorbances of the treated and untreated cells were denoted as A_1 and A_0, respectively.

2.9. Tyrosinase activity assay in A375 cells

The inhibitive effect of PtNPs on the activity of tyrosinase was determined by spectrophotometric. Cells were grown in cell culture dishes (35 × 10 mm) and treated with different concentrations of PtNPs for 24 h. The cells were washed twice by using PBS and added lysis buffer containing 1% Triton X-100 with PMSF. Then the cells were frozen at −20 °C for 30 min, thawed at 4 °C, harvested and centrifuged at 12000 rpm for 30 min. The concentration of the protein in collected lysate was quantified with a bicinchoninic acid assay kit (BCA, Solarbio, Beijing, China) and adjusted consistently by lysis buffer. Tyrosinase activity assay reaction system, including cellular extracts (80 μL), 200 μL of 4 mg/mL levodopa and sodium phosphate buffer (pH = 6.8). They were mixed and reacted at 37 °C for 3 h in the dark. Absorbance at 490 nm was recorded by ScanDrop, and the relative tyrosinase activity was represented as the percentage of PtNPs-treated cells against untreated cells. The activity of tyrosinase was calculated according to the equation below:

$$Tyrosinase Activity(\%) = T_1/T_0 \times 100$$

where T_1 and T_0 were the absorbance values of treated cells and control, respectively.

2.10. UVB irradiation and melanin content assay

A375 cells were grown in cell culture dishes (35 × 10 mm) and incubated with PtNPs for 24 h. Then, the culture medium was substituted by 500 μL of PBS, and cells were irradiated with UVB light (80 mJ/cm²). The UVB strength was determined by UV intensity meter (UV-340A, Luchang Electronic Enterprise, Taipei, Taiwan). After UVB treatment, cells were cultured for additional 24 h. For measurement of melanin content, cells were cleaned twice with PBS and lysed with RIPA lysis buffer containing PMSF. The collected lysates were centrifuged at 12,000 rpm for 20 min, and the protein concentration was determined by BCA method. The supernatants were added to 150 μL of NaOH (1 M, containing 10% DMSO) and reacted at 60 °C for 30 min. The absorbance of the reacted solution at 405 nm was recorded by ScanDrop. The melanin content was calculated as the equation below:

$$Melanin\ content(\%) = A_1/A_0 \times 100$$

where A_0 and A_1 are the absorbance values of untreated and treated cells, respectively.

2.11. Western blot analysis

After HFF-1 cells were incubated with different concentrations of PtNPs for 72 h, their proteins were extricated with RIPA lysis buffer containing protease inhibitors to gather the cell lysate. Protein concentration was measured by the BCA method and adjusted consistently by using PBS. The proteins were separated by sodium dodecyl sulfate–polyacrylamide gel electrophoresis (SDS-PAGE) and transferred to polyvinylidene fluoride (PVDF) membranes activated by methanol. The membranes were sealed with 5% skim milk powder for 2 h and incubated overnight with primary antibodies to collagen I, TGF-β, Smad3, pSmad3 or β-actin at 4 °C. Then these primary antibodies were washed out, the membranes were incubated with horseradish peroxidase-labeled secondary antibodies for another 2 h. Eventually, the targeted proteins were detected by Superstar ECL (BOSTER, Wuhan, China) western blotting detection reagents and visualized by the ChemiDoc MP Imaging system.

2.12. Statistical analysis

All experiments were repeated no less than three times, and the final data were presented as the mean ± standard deviation (SD). Two group comparisons were performed by independent-sample *t*-test, and multiple different groups were compared by ANOVA. $P < 0.05$ was denoted as statistically significant.

3. Results

3.1. UV–visible spectroscopy analysis

The green synthesis of PtNPs was through the reaction of H_2PtCl_6 and *N. tetragona* extract. During the reacting process, the color of the solution gradually changed from pale yellow to brown or even black, indicating the synthesis of PtNPs. UV–visible spectroscopy is commonly made use of demon-

strating the production and stability of metal NPs/colloidal particles. The UV–vis optical absorption results of Fig. 1 also confirmed the synthesis of PtNPs. H_2PtCl_6 solution has an absorption peak at approximately 260 nm due to the presence of $PtCl_6^{2-}$ ions in water, and the absorption peak of the *N. tetragona* extract was at approximately 266 nm. With the formation of PtNPs, these two absorption peaks disappeared, and a sharp peak was obtained at about 230 nm in the two samples (L1-PtNPs and L4-PtNPs), which indicated that the precursor salt was completely reduced to zero-valent platinum nanoparticles. Other than, the existence of a sharp surface plasmon resonance (SPR) absorption peak at 230 nm confirmed that small-sized PtNPs was embraced in the solution. The UV absorption peak of L4-PtNPs is sharper than that of L1-PtNPs, which showed the size of L4-PtNPs might be smaller (Eramabadi et al., 2020).

3.2. Transmission electron microscopy (TEM) analysis

TEM analysis was performed to confirm the size and shape of PtNPs (Fig. 2). Results showed that PtNPs were evenly distributed and surrounded by the *N. tetragona* extract, indicating that the *N. tetragona* extract acts as a sealing agent to separate PtNPs from the aggregation (Jiao et al., 2021). PSD (particle size distribution) plots were obtained by measuring no less than 100 PtNPs for each sample. The average particle sizes of PtNPs were 4.04 ± 1.31 nm (Fig. 2B) and 2.21 ± 0.80 nm (Fig. 2D) when prepared with H_2PtCl_6 and *N. tetragona* extracts at ratios of 1:1 (L1-PtNPs) and 1:4 (L4-PtNPs), respectively. The results displayed the average particle size of L4-PtNPs was smaller than that of L1-PtNPs. TEM further testified that we obtained two PtNPs with different particle diameters by changing the ratio of *N. tetragona* extract.

3.3. X-ray diffraction (XRD) study

XRD pattern was performed to determine the crystal structure and phase purity of the prepared samples. In the results of Fig. 3, the diffraction peaks at 2 theta values of 39.76°,
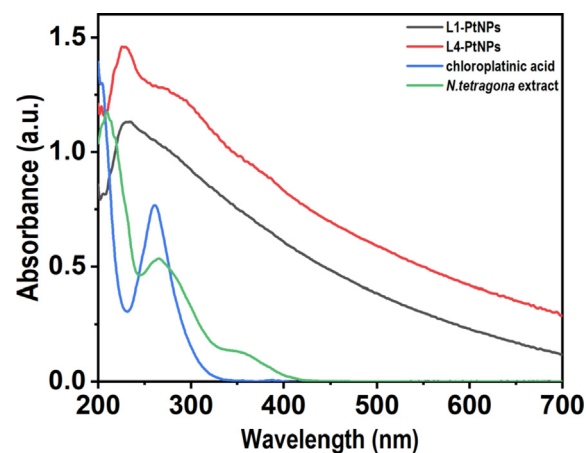
Fig. 1 UV–visible absorption spectra of reduced PtNPs. Blue, green, black and red colors represent the UV absorption peaks of the *N. tetragona* extract, chloroplatinic acid, L1-PtNPs and L4-PtNPs, respectively.
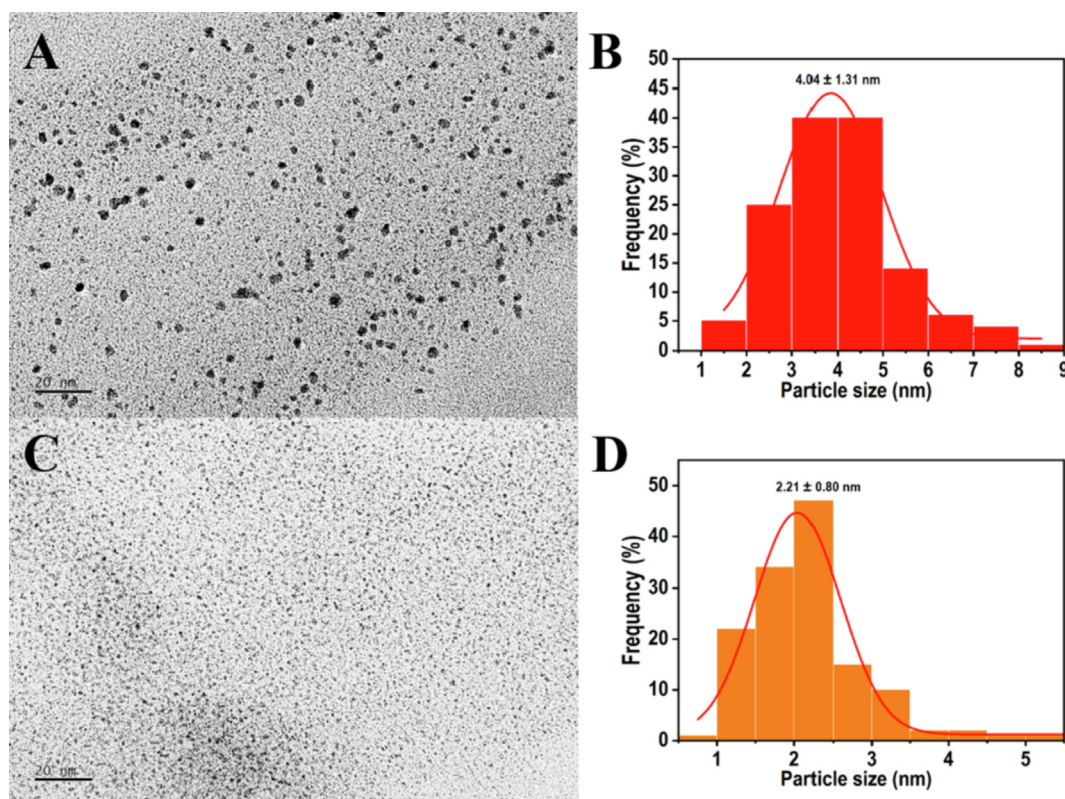
Fig. 2 TEM micrographs of PtNPs green synthesized with H_2PtCl_6 and *N. tetragona* extracts at ratios of 1:1 (L1-PtNPs) and 1:4 (L4-PtNPs). **A, B** and **C, D** represent the TEM of L1-PtNPs and L4-PtNPs, respectively.

46.24°, 67.45° and 81.28° correspond to the index planes (1 1 1), (2 0 0), (2 2 0) and (3 1 1) of the cubic structure of metallic platinum (JCPDS #04–0802), indicating the high-purity face-centered cubic (fcc) crystals of the prepared PtNPs. XRD revealed that a strong Bragg reflection lattice peak was observed on the (1 1 1) plane. Therefore, PtNPs with index (1 1 1) orientation tiled on the planar surface. However, the closest reflection assimilated to (2 0 0), (2 2 0) and (3 1 1) with a specific lattice spacing, which displayed the different morphologies that exist in the samples. Meanwhile, the 2θ values of the wide peaks indirectly indicated the smaller particles of

PtNPs (Zheng et al., 2013; Yu et al., 2019). The particle size of formed PtNPs was calculated by Debye-Scherer equation.

$$D = k\lambda/(\beta \cos\theta)$$

where *d* represents the average crystallite size, *k* represents the Scheeler constant ($k = 0.9$), λ determines the X-ray wavelength ($\lambda = 0.154$ nm), *β* represents the broadening measured in radians, and θ determines the Bragg angle (Mahdavi et al., 2013). The average crystallite sizes of L1-PtNPs and L4-PtNPs calculated by Scherrer equation were 2.82 nm and 1.95 nm respectively.

3.4. FTIR spectroscopy study

FTIR spectroscopy was performed to determine biomolecules that affect the reduction and stability of PtNPs. In Fig. 4, it can be seen that the FTIR spectra of L1-PtNPs and L4-PtNPs samples are hardly different, and there is a clear similarity with that of *N. tetragona* extract. The main stretching vibrations of O—H bonds at 3000–3500 cm^{-1} indicated the existence of phenols, flavonoids and other compounds. In addition, a slight shift appeared in the belt, confirming that the existence of carbonyl groups in the *N. tetragona* extract was stable and covered the formation of PtNPs. Except for the stretching vibrations of O—H bonds, the presence of C—H bonds in the regions of 2936 and 2930 cm^{-1} is prominent. The bands appearing at 1609 and 1612 cm^{-1} represented the vibration of the C=O bonds, which is the typical structure of flavonoids. In the range of 1500–1600 cm^{-1}, the subsistence of C—C in the ring aromatic bond was attributed to aromatic

Fig. 3 XRD pattern of *N. tetragona* extract-mediated PtNPs.
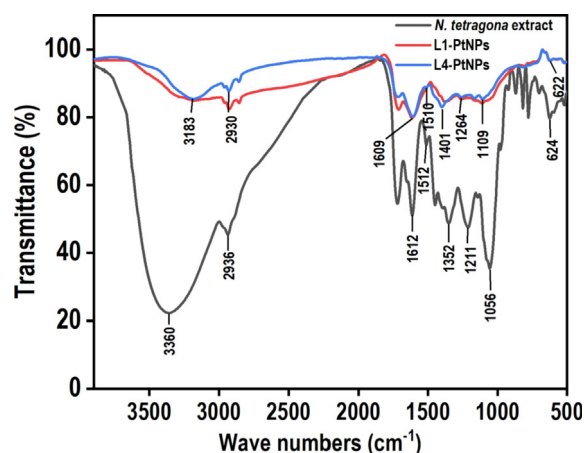
Fig. 4 FTIR spectrum of *N. tetragona* extract and green synthesized PtNPs. Black, red and blue colors represent the FTIR spectra of the *N. tetragona* extract, L1-PtNPs and L4-PtNPs, respectively.

groups existent in the *N. tetragona* extract. In these three spectra, the C—C bond aromatic extensions in the range of 1400–1500 cm^{-1} are essential for the predominant aromatic backbone contained in the *N. tetragona* extract. In addition, the C—O—C stretch moved from 1264 cm^{-1} to 1211 cm^{-1} after PtNPs in this area were capped. The band at around 600 cm^{-1} indicated the existence of an R-CH group, and the band of three samples at approximately 1380 cm^{-1} demonstrated similarity to the C—N stretching vibrations in aromatic amines. It is well known that proteins can bind to PtNPs through free amines and carboxyl groups, which contributes to the preparation and stability of PtNPs.

3.5. Effect of PtNPs on antioxidant activity in vitro

FRAP method is generally utilized to evaluate the antioxidant ability. FRAP assay involves appraising the capacity of the test substance to restore Fe^{3+} to Fe^{2+} in the existence of TPTZ to produce a strong blue Fe^{2+}-TPTZ complex. Table 1 showed the results for ferric-ion-reducing abilities of PtNPs after FRAP analysis. The antioxidant activity of L4-PtNPs (IC50 value is 2.98 ± 0.04 μg/mL) was eminently heftier than L1-PtNPs ($P < 0.05$), indicating that L4-PtNPs displayed better reducing activity.

In the determination of ABTS, blue/green ABTS•+ chromophore is formed by the response of ABTS and potassium persulfate. Antioxidants restore the radical of ABTS•+ to ABTS. The results of the ABTS free radical scavenging ability of PtNPs samples presented that L4-PtNPs had higher ABTS

radical-scavenging activity than L1-PtNPs (Table 1), which is consistent with the results of FRAP assay.

3.6. PtNPs inhibit tyrosinase activity

Tyrosinase is a crucial regulative enzyme for the production of melanin, and determining its activity has always been the first stride to study the decrement pigmentation mechanism of elected chemical agents (Hu et al., 2015). Therefore, mushroom tyrosinase activity *in vitro* was tested to determine whether PtNPs inhibit melanin synthesis by inhibiting tyrosinase activity. In Fig. 5A, *N. tetragona* extract showed no obvious inhibitive effect on the activity of tyrosinase, and PtNPs showed a strong inhibitive effect on the activity of tyrosinase. The tyrosinase activity decreased in a dose-dependent manner with increasing PtNPs concentration. The IC$_{50}$ values of L1-PtNPs and L4-PtNPs were 4.04 ± 0.70 μg/mL and 9.72 ± 0.48 μg/mL, respectively, indicating that the inhibitory effect of L1-PtNPs on tyrosinase activity was superior to L4-PtNPs. In addition, the IC$_{50}$ values of L1-PtNPs and L4-PtNPs on tyrosinase activity were lower than the recognized standard whitening agent kojic acid (IC$_{50}$ value was 77.89 ± 4.84 μg/mL), respectively.

The cytotoxicity of PtNPs was first evaluated by the CCK-8 assay, the results displayed that L1-PtNPs and L4-PtNPs did not reduce the growth of A375 cells at 5 μg/mL after 24 h (Fig. 5B), and *N. tetragona* extract did not reduce the growth of A375 cells at 100 μg/mL (Fig. 5C). Aiming to further fix upon the effect of PtNPs on tyrosinase activity, its effect on tyrosinase activity in A375 cells was measured. In the results of Fig. 5D, *N. tetragona* extract did not significantly inhibit intracellular tyrosinase activity in A375 cells, and both L1-PtNPs and L4-PtNPs significantly inhibited intracellular tyrosinase activity in A375 cells at concentrations of 0.1, 0.5 and 1 μg/mL, but there was no distinct difference between them. The effects of PtNPs on UVB-induced melanin synthesis was next investigated in A375 cells to verify its whitening effect. Results exhibited that *N. tetragona* extract did not reduce melanin synthesis, and PtNPs significantly inhibited intracellular melanin production contrasted to that of the UVB-treated control (Fig. 5E). However, the inhibitory effects on UVB-induced melanin production of L1-PtNPs and L4-PtNPs were not prominently different, which is consistent with their effects on tyrosinase activity.

3.7. PtNPs promote collagen I synthesis

Collagen provides elasticity and strength to the skin, and degradation of collagen will cause skin aging (Kim et al., 2015). To determine whether PtNPs affect collagen synthesis,

Table 1 Antioxidant capacity values of L1-PtNPs and L4-PtNPs.

Sample	FRAP		ABTS	
	IC50 value (μg/mL)	mg Trolox/g	IC50 value (μg/mL)	mg Trolox/g
L1-PtNPs	7.89 ± 0.19	322.00 ± 2.57[b]	7.85 ± 0.20	503.56 ± 8.77[b]
L4-PtNPs	2.98 ± 0.04	854.20 ± 19.93[a]	1.23 ± 0.03	3212.91 ± 32.39[a]

Notes: Data are presented as the mean $\pm$ SD of replicate experiments; different numbers in the same column with different letters as superscript are significantly ($P < 0.05$) different.
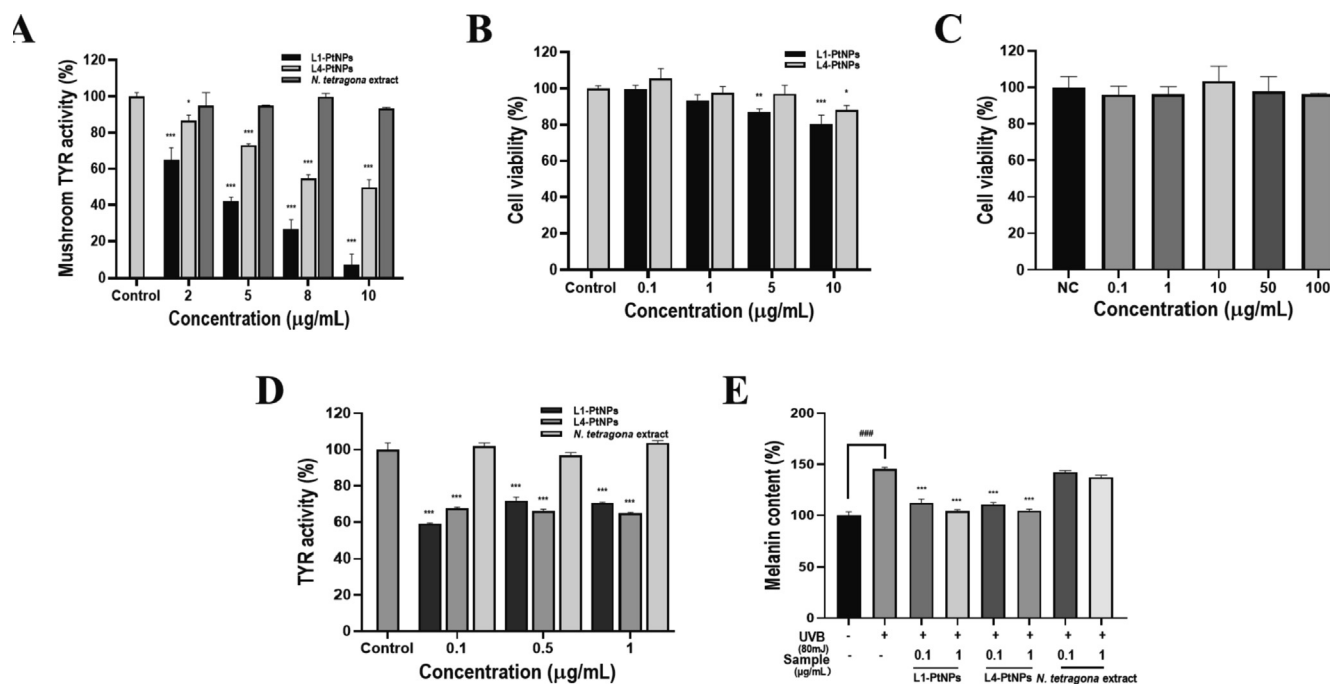
Fig. 5 Green synthesized L1-PtNPs and L4-PtNPs can inhibit tyrosinase activity. **A.** Effects of PtNPs and *N. tetragona* extract on mushroom tyrosinase activity (*$P < 0.05$, **$P < 0.01$, ***$P < 0.001$). **B.** Effects of PtNPs on A375 cell viability (*$P < 0.05$, **$P < 0.01$, ***$P < 0.001$). **C.** Effects of PtNPs and *N. tetragona* extract on tyrosinase activity in A375 cells. **D.** Effect of PtNPs and *N. tetragona* extract on UVB-induced melanin biosynthesis in A375 cells. (#$P < 0.05$, ##$P < 0.01$, ###$P < 0.001$) compared with the control; (*$P < 0.05$, **$P < 0.01$, ***$P < 0.001$) compared with UVB-treated cells. Data are represented as mean ± SD of replicate experiments.

we performed Western blot analysis. The effect of PtNPs on the viability of HFF-1 cells was determined before the Western blot analysis, both L1-PtNPs and L4-PtNPs had no cytotoxic effect on HFF-1 cells at 2.5 µg/ml (Fig. 6F). Therefore, follow-up experiments were carried out on HFF-1 cells when PtNPs was below 2.5 µg/mL. In Fig. 6 results, when the concentration of L1-PtNPs was 0.1 µg/mL, the expression of collagen I did not change substantially in HFF-1 cells. However, after treatment with 1 µg/mL L1-PtNPs, 0.1 and 1 µg/mL L4-PtNPs, collagen I synthesis was distinctly increased. The results indicated that PtNPs can promote collagen I production in HFF-1 cells, and L4-PtNPs was better.

The TGF-β/Smad pathway is the main signaling pathway for dermal collagen production, so whether it is involved in the expression of collagen I induced by green synthetic PtNPs in HFF-1 cells was evaluated. After treatment with 0.1 µg/mL L1-PtNPs, the expression of TGF-β did not change significantly. When the L1-PtNPs was 1 µg/mL and the L4-PtNPs were 0.1 and 1 µg/mL, the TGF-β expression level clearly increased in HFF-1 cells. This is consistent with the expression of collagen I. In order to further clarify the molecular pathways of collagen I production induced by green synthetized PtNPs, the effect of PtNPs on Smad3 was determined and results showed no change in the expression of Smad3 proteins. Then Smad3 phosphorylation was measured and results showed that Smad3 proteins were phosphorylated in PtNPs-treated HFF-1 cells (Fig. 6). The change in its expression was the same as collagen I and TGF-β. These results displayed that HFF-1 cells treated with PtNPs can promote the synthesis of collagen I by activating TGF-β/Smad signaling pathway.

4. Discussion

In recent years, the green synthesis of metal nanoparticles by biological methods and their application in biomedicine have received widespread attention. Compared with traditional chemical and physical synthesis methods, green biosynthetic metal NPs have been widely studied by researchers due to the environment-friendly synthesis methods and the biocompatibility of the synthesized metal NPs (Pedone et al., 2017; Jiao et al., 2021). However, the subsequent processing of intracellular biosynthetic NPs is usually difficult, and the microorganisms that biosynthesize NPs must be screened extensively. In contrast to microbial methods, plant-based biosynthesis of NPs is not only simple, effective and rapid, but also more controllable for the shape and size of metal NPs (Zheng et al., 2013). In addition, studies have shown that the activities of reducing sugars, flavonoids and proteins in plant extracts are closely related to the biological reduction of silver or gold ions, and there is a growing list of reports indicating that green synthetic metal NPs with plant extracts have certain characteristics of plant active substances (Yang et al., 2017; Huang et al., 2011; Zhou et al., 2010). In this study, PtNPs were synthesized by *N. tetragona* extract, and their biological effects on skin were explored.

Song *et al.* reported that the average size of PtNPs decreases as the concentration of *Diopyros kaki* leaf extract increases in the biosynthesis of platinum nanoparticles (Song et al., 2010). Similarly, the study on the size-tunable green synthesis of platinum nanoparticles using chlorogenic acid clearly showed that the increase in CGA leads to the decrease of the
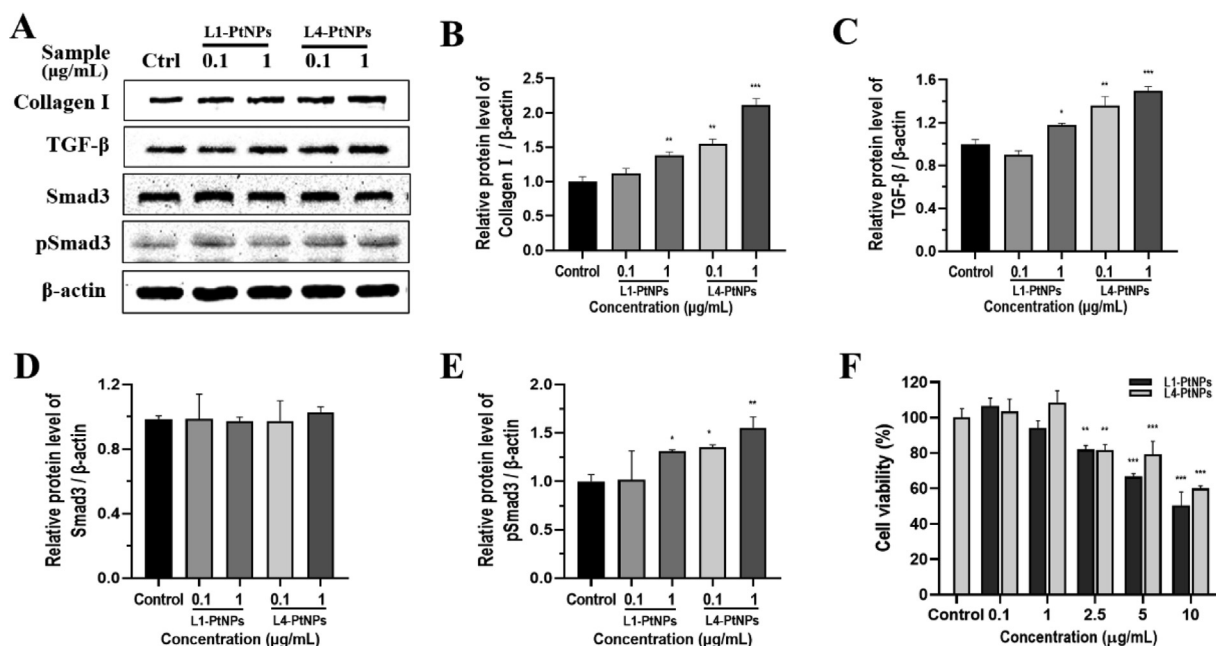
Fig. 6 Green synthesized L1-PtNPs and L4-PtNPs can promote collagen I by activating TGF β/Smad signaling pathway. **A-E.** Effects of PtNPs on collagen I, TGF β, Smad3 and pSmad3 expression in HFF-1 cells. **F.** Effects of PtNPs on HFF-1 cells viability. Data are represented as mean ± SD of replicate experiments (*$P < 0.05$, **$P < 0.01$, ***$P < 0.001$).

PtNPs' size (Chen et al., 2021). In our research, PtNPs with two particle sizes were obtained by adding *N. tetragona* extract to reduce the size of PtNPs. Then the two prepared PtNPs was characterized. The UV absorption peak of L4-PtNPs was sharper than that of L1-PtNPs, and TEM analysis showed the sizes of L4-PtNPs was smaller, which is consistent with the smallest PtNPs having the sharpest peak of in Eramabadi et al.'s report (Eramabadi et al., 2020). Moreover, research has shown that the different absorbances of PtNPs solutions at the same concentration also represent their different sizes, which is in accordance with our results (Zheng et al., 2013). The XRD data analysis demonstrated that the 2θ value of the broad peak also indirectly represents the smaller PtNPs particles, which is in good agreement with the results reported in the relevant literature (Zheng et al., 2013; Yu et al., 2019). FTIR further indicated that the PtNPs was mainly composed of phenols and flavonoids, which act as a reducing agent and a sealing agent. This is similar to Selvi et al.'s report that phenols and flavonoids in the *Tragia involucrat* extract showed excellent reducing and stabilizing effects in the synthesis of PtNPs (Selvi et al., 2020).

Green synthetic PtNPs might have potential application prospects in whitening and anti-aging in the field of skin. Melanin is an essential factor that determines the color of human skin, eyes and hair. Melanin production is a stress reaction of melanocytes that can lead to melanosis, such as freckles, brown spots, age spots and even melanoma (Wang et al., 2013; Hua et al., 2020). The biosynthesis of melanin constructs a various of biochemical responses triggered by the hydroxylation of tyrosine catalyzed by tyrosinase *in vivo*, and tyrosinase acts a vital role in this list of responses (Sun et al., 2017). Therefore, controlling tyrosinase activity can control the amount of melanin production to achieve the effect of skin whitening. This study demonstrates that green synthetic PtNPs

can not only decrease the activity of mushroom tyrosinase *in vitro*, but also reduce the activity of tyrosinase and UVB-induced melanin production in A375 cells. Collagen, especially collagen I, is the most abundant protein in human skin, which is closely related to skin aging (Park et al., 2016). In addition, anti-free radical activity is also a potentially effective strategy to delay skin aging (Kim et al., 2015). TGF-β is the primary activator of collagen I synthesis in skin fibroblasts. The Smad signaling pathway acts a dominant role in the transcriptional reaction of TGF-β signaling, such as activating collagen I gene expression (Kim et al., 2017). M. Hashimoto et al reported that PtNPs can inhibit the activity of matrix metalloproteinase (MMP) -1, -2 and -9 (Hashimoto et al., 2016), while latent MMP-1, -2, and -9 derived from dermal fibroblasts could be greatly activated by MMP-3 and ultimately initiate degradation collagen I (Kim et al., 2015). In this study, we indicated green synthetic PtNPs perspicuously up-regulated the expression of collagen I, which further confirmed the view of M. Hashimoto et al. Moreover, we determined that the expression of TGF-β was up-regulated, and Smad3 was phosphorylated in HFF-1 cells treated with green synthetic PtNPs, illustrating that it promotes the synthesis of collagen I by stimulating the TGF-β/Smad signaling pathway. This research also indicated that L4-PtNPs can promote collagen I synthesis more than L1-PtNPs, as well as higher activity of TGF-β/Smad signaling pathways. Not only that, the green synthetic PtNPs also shows high activity in scavenging free radicals *in vitro*. FRAP and ABTS assay both indicated that PtNPs can scavenge free radicals very well, and L4-PtNPs have better oxidation resistance. Previously, there was no research demonstrating that PtNPs has whitening and anti-aging effects, but there have been reports that PtNPs can be used in food additives and cosmetics (Pedone et al., 2017; Konieczny et al., 2013). This study illustrates for the first time that green synthesized PtNPs can

achieve skin whitening and anti-aging effects by inhibiting tyrosinase activity, promoting collagen I synthesis and anti-free radical.

AgNPs is one of the most commercialized NPs and is widely used in household products, textiles, therapeutics and cosmetics. However, much evidence has shown that AgNPs has high cytotoxicity (Szmyd et al., 2013). These data provided by this research showed that green synthetic PtNPs has no obvious toxic effect on HFF-1 and A375 cells, and it provides evidence for people to consider applying PtNPs to skin protection. It must be pointed out that because the skin acts as a barrier to potentially dangerous substances, the effects observed *in vitro* may be different from the effects of NPs on human skin. Further *in vivo* studies are particularly consequential to clarify this problem. There is already evidence that the direct use of NPs on the skin can only penetrate the final stage of the exfoliation layer, the skin layer (Campbell et al., 2012). Therefore, we can consider whether PtNPs can be used in skin protection instead of the more toxic AgNPs.

5. Conclusion

This study proposes a simple and green method for synthesizing PtNPs with adjustable size using *N. tetragona* extract as a reducing agent and capping agent. The method obtains PtNPs of two different sizes by changing the ratio of H_2PtCl_6 and *N. tetragona* extract. And the green synthesized PtNPs are small in particle size and well-dispersion. This work also explores the biological effects of green-synthesized PtNPs with two particle sizes in the skin field. Results showed that the two PtNPs can significantly reduce tyrosinase activity *in vitro* and in A375 cells and can reduce UVB-induced melanin production in A375 cells. In addition, they can increase collagen I synthesis by activating the TGF β/Smad signaling pathway in HFF-1 cells. From these studies, the green synthesized PtNPs seems to be promising for skin whitening and antiaging.

Declaration of Competing Interest

The authors declare that they have no known competing financial interests or personal relationships that could have appeared to influence the work reported in this paper.

Acknowledgement

References

Al-Qudah, T., Mahmood, S.H., Abu-Zurayk, R., Shibli, R., Khalaf, A., Lambat, T.L., Chaudhary, R.G., 2022. Nanotechnology applications in plant tissue culture and molecular genetics: a holistic approach. Curr. Nanosci. 18, 442–464.

Alvarez, R.A.B., Cortez-Valadez, M., Bueno, L.O.N., Hurtado, R.B., Rocha-Rocha, O., Delgado-Beleno, Y., Martinez-Nunez, C.E., Serrano-Corrales, L.I., Arizpe-Chavez, H., Flores-Acosta, M., 2016. Vibrational properties of gold nanoparticles obtained by green synthesis. Physica E 84, 191–195.

Bhardwaj, K., Dhanjal, D.S., Sharma, A., Nepovimova, E., Kalia, A., Thakur, S., Bhardwaj, S., Chopra, C., Singh, R., Verma, R., Kumar, D., Bhardwaj, P., Kuca, K., 2020. Conifer-derived metallic nanoparticles: green synthesis and biological applications. Int. J. Mol. Sci. 21, 9028–9049.

Campbell, C.S., Contreras-Rojas, L.R., Delgado-Charro, M.B., Guy, R.H., 2012. Objective assessment of nanoparticle disposition in mammalian skin after topical exposure. J. Control. Release 162, 201–207.

Castro, L., Blazquez, M.L., Gonzalez, F., Munoz, J.A., Ballester, A., 2015. Biosynthesis of silver and platinum nanoparticles using orange peel extract: characterisation and applications. IET Nanobiotechnol. 9, 252–258.

Chaudhary, R.G., Bhusari, G.S., Tiple, A.D., Rai, A.R., Somkuvar, S. R., Potbhare, A.K., Lambat, T.L., Ingle, P.P., Abdala, A.A., 2019. Metal/metal oxide nanoparticles: toxicity, applications, and future prospects. Curr. Pharm. Design 25, 4013–4029.

Chen, R., Wu, S., Meng, C., 2021. Size-tunable green synthesis of platinum nanoparticles using chlorogenic acid. Res. Chem. Intermed. 47, 1775–1787.

Chowdhury, A., Nosoudi, N., Karamched, S., Parasaram, V., Vyavahare, N., 2021. Polyphenol treatments increase elastin and collagen deposition by human dermal fibroblasts; implications to improve skin health. J. Dermatol. Sci. 102, 94–100.

El-Seedi, H.R., El-Shabasy, R.M., Khalifa, S.A.M., Saeed, A., Shah, A., Shah, R., Iftikhar, F.J., Abdel-Daim, M.M., Omri, A., Hajrahand, N.H., Sabir, J.S.M., Zou, X.B., Halabi, M.F., Sarhan, W., Guo, W.S., 2019. Metal nanoparticles fabricated by green chemistry using natural extracts: biosynthesis, mechanisms, and applications. Rsc Adv. 9, 24539–24559.

Eramabadi, P., Masoudi, M., Makhdoumi, A., Mashreghi, M., 2020. Microbial cell lysate supernatant (CLS) alteration impact on platinum nanoparticles fabrication, characterization, antioxidant and antibacterial activity. Mater. Sci. Eng. C Mater. Biol. Appl. 117, 111292–111303.

Gahlawat, G., Choudhury, A.R., 2019. A review on the biosynthesis of metal and metal salt nanoparticles by microbes. Rsc Adv. 9, 12944–12967.

Hashimoto, M., Kawai, K., Kawakami, H., Imazato, S., 2016. Matrix metalloproteases inhibition and biocompatibility of gold and platinum nanoparticles. J. Biomed. Mater. Res. A 104, 209–217.

Hsu, J.Y., Lin, H.H., Li, T.S., Tseng, C.Y., Wong, Y., Chen, J.H., 2020. Anti-melanogenesis effects of lotus seedpod in vitro and in vivo. Nutrients 12, 3535–3551.

Hu, S., Zheng, Z., Zhang, X., Chen, F., Wang, M., 2015. Oxyresveratrol and trans-dihydromorin from the twigs of Cudrania tricuspidata as hypopigmenting agents against melanogenesis. J. Funct. Foods 13, 375–383.

Hua, Y., Ma, C., Wei, T., Zhang, L., Shen, J., 2020. Collagen/Chitosan complexes: preparation, antioxidant activity, tyrosinase inhibition activity, and melanin synthesis. Int. J. Mol. Sci. 21, 313–327.

Huang, J., Wang, W., Lin, L., Li, Q., Lin, W., Li, M., Mann, S., 2009. A general strategy for the biosynthesis of gold nanoparticles by traditional Chinese medicines and their potential application as catalysts. Chem. Asian J. 4, 1050–1054.

Huang, J.L., Zhan, G.W., Zheng, B.Y., Sun, D.H., Lu, F.F., Lin, Y., Chen, H.M., Zheng, Z.D., Zheng, Y.M., Li, Q.B., 2011. Biogenic silver nanoparticles by Cacumen Platycladi extract: synthesis, formation mechanism, and antibacterial activity. Ind. Eng. Chem. Res. 50, 9095–9106.

Jiao, Y., Wang, X., Chen, J.H., 2021. Biofabrication of AuNPs using Coriandrum sativum leaf extract and their antioxidant, analgesic activity. Sci. Total Environ. 767, 144914–144922.

Khan, A.U., Malik, N., Khan, M., Cho, M., Khan, M.M.M., 2018. Fungi-assisted silver nanoparticle synthesis and their applications. Bioproc. Biosyst. Eng. 41, 1–20.

Kim, C.R., Kim, Y.M., Lee, M.K., Kim, I.H., Choi, Y.H., Nam, T.J., 2017. Pyropia yezoensis peptide promotes collagen synthesis by activating the TGF-beta/Smad signaling pathway in the human dermal fibroblast cell line Hs27. Int. J. Mol. Med. 39, 31–38.

Kim, M., Park, Y.G., Lee, H.J., Lim, S.J., Nho, C.W., 2015. Youngiasides A and C Isolated from Youngia denticulatum inhibit UVB-induced MMP expression and promote Type I Procollagen production via repression of MAPK/AP-1/NF-kappaB and activation of AMPK/Nrf2 in HaCaT cells and human dermal fibroblasts. J. Agric. Food Chem. 63, 5428–5438.

Konieczny, P., Goralczyk, A.G., Szmyd, R., Skalniak, L., Koziel, J., Filon, F.L., Crosera, M., Cierniak, A., Zuba-Surma, E.K., Borowczyk, J., Laczna, E., Drukala, J., Pyza, E., Semik, D., Woznicka, O., Klein, A., Jura, J., 2013. Effects triggered by platinum nanoparticles on primary keratinocytes. Int. J. Nanomed. 8, 3963–3975.

Mahdavi, M., Namvar, F., Ahmad, M.B., Mohamad, R., 2013. Green biosynthesis and characterization of magnetic iron oxide (Fe(3)O (4)) nanoparticles using seaweed (Sargassum muticum) aqueous extract. Molecules 18, 5954–5964.

Mondal, A., Umekar, M.S., Bhusari, G.S., Chouke, P.B., Lambat, T., Mondal, S., Chaudhary, R.G., Mahmood, S.H., 2021. Biogenic synthesis of metal/metal oxide nanostructured materials. Curr. Pharm. Biotechno. 22, 1782–1793.

Mukherjee, P.K., Saha, K., Das, J., Pal, M., Saha, B.P., 1997. Studies on the anti-inflammatory activity of rhizomes of Nelumbo nucifera. Planta Med. 63, 367–369.

Park, S.H., Jeong, S.H., Kim, S.W., 2016. β-Lapachone regulates the transforming growth factor-beta-smad signaling pathway associated with collagen biosynthesis in human dermal fibroblasts. Biol. Pharm. Bull. 39, 524–531.

Pedone, D., Moglianetti, M., De Luca, E., Bardi, G., Pompa, P.P., 2017. Platinum nanoparticles in nanobiomedicine. Chem. Soc. Rev. 46, 4951–4975.

Rajagopal, K., Sasikala, K., 2008. Antihyperglycaemic and antihyperlipidaemic effects of Nymphaea stellata in diabetic rats alloxan-induced. Singap. Med. J. 49, 137–141.

Samadi, A., Klingberg, H., Jauffred, L., Kjaer, A., Bendix, P.M., Oddershede, L.B., 2018. Platinum nanoparticles: a non-toxic, effective and thermally stable alternative plasmonic material for cancer therapy and bioengineering. Nanoscale 10, 9097–9107.

Selvi, A.M., Palanisamy, S., Jeyanthi, S., Vinosha, M., Mohandoss, S., Tabarsa, M., You, S., Kannapiran, E., Prabhu, N.M., 2020. Synthesis of Tragia involucrata mediated platinum nanoparticles for comprehensive therapeutic applications: antioxidant, antibacterial and mitochondria-associated apoptosis in HeLa cells. Process Biochem. 98, 21–33.

Siddiqi, K.S., Husen, A., 2016. Green synthesis, characterization and uses of palladium/platinum nanoparticles. Nanoscale Res. Lett. 11, 482–494.

Siddiqi, K.S., Husen, A., Rao, R.A.K., 2018. A review on biosynthesis of silver nanoparticles and their biocidal properties. J. Nanobiotechnol. 16, 14–41.

Song, J.Y., Kwon, E.Y., Kim, B.S., 2010. Biological synthesis of platinum nanoparticles using Diopyros kaki leaf extract. Bioproc. Biosyst. Eng. 33, 159–164.

Sun, L., Guo, Y., Zhang, Y., Zhuang, Y., 2017. Antioxidant and antityrosinase activities of phenolic extracts from rape bee pollen and inhibitory melanogenesis by cAMP/MITF/TYR pathway in B16 Mouse melanoma cells. Front. Pharmacol. 8, 104–112.

Szmyd, R., Goralczyk, A.G., Skalniak, L., Cierniak, A., Lipert, B., Filon, F.L., Crosera, M., Borowczyk, J., Laczna, E., Drukala, J., Klein, A., Jura, J., 2013. Effect of silver nanoparticles on human primary keratinocytes. Biol. Chem. 394, 113–123.

Venu, R., Ramulu, T.S., Anandakumar, S., Rani, V.S., Kim, C.G., 2011. Bio-directed synthesis of platinum nanoparticles using aqueous honey solutions and their catalytic applications. Colloids Surf. A: Physicochem. Eng. Asp. 384, 733–738.

Wang, H., Zhang, S., Wu, C., Zhang, Z., Qin, T., 2013. Melanocytomas of the central nervous system: a clinicopathological and molecular study. Eur. J. Clin. Invest. 43, 809–815.

Yang, C., Wang, M., Zhou, J., Chi, Q., 2017. Bio-synthesis of peppermint leaf extract polyphenols capped nano-platinum and their in-vitro cytotoxicity towards colon cancer cell lines (HCT 116). Mater. Sci. Eng. C Mater. Biol. Appl. 77, 1012–1016.

Yu, X., Yuan, L., Zhu, N., Wang, K., Xia, Y., 2019. Fabrication of antimicrobial curcumin stabilized platinum nanoparticles and their anti-liver fibrosis activity for potential use in nursing care. J. Photochem. Photobiol. B 195, 27–32.

Zeng, Y., Guo, L.P., Chen, B.D., Hao, Z.P., Wang, J.Y., Huang, L.Q., Yang, G., Cui, X.M., Yang, L., Wu, Z.X., Chen, M.L., Zhang, Y., 2013. Arbuscular mycorrhizal symbiosis and active ingredients of medicinal plants: current research status and prospectives. Mycorrhiza 23, 253–265.

Zheng, B., Kong, T., Jing, X., Odoom-Wubah, T., Li, X., Sun, D., Lu, F., Zheng, Y., Huang, J., Li, Q., 2013. Plant-mediated synthesis of platinum nanoparticles and its bioreductive mechanism. J. Colloid Interface Sci. 396, 138–145.

Zhou, Y., Lin, W.S., Huang, J.L., Wang, W.T., Gao, Y.X., Lin, L.Q., Li, Q.B., Lin, L., Du, M.M., 2010. Biosynthesis of gold nanoparticles by foliar broths: roles of biocompounds and other attributes of the extracts. Nanoscale Res. Lett. 5, 1351–1359.